LBL-19501
UC-21 c.2

Lawrence Berkeley Laboratory

UNIVERSITY OF CALIFORNIA

Accelerator & Fusion Research Division

DOCUMENTS SECTION

HEAVY ION FUSION HALF YEAR REPORT
October 1, 1984-March 30, 1985

Heavy Ion Fusion Staff

June 1985

TWO-WEEK LOAN COPY
This is a Library Circulating Copy which may be borrowed for two weeks.

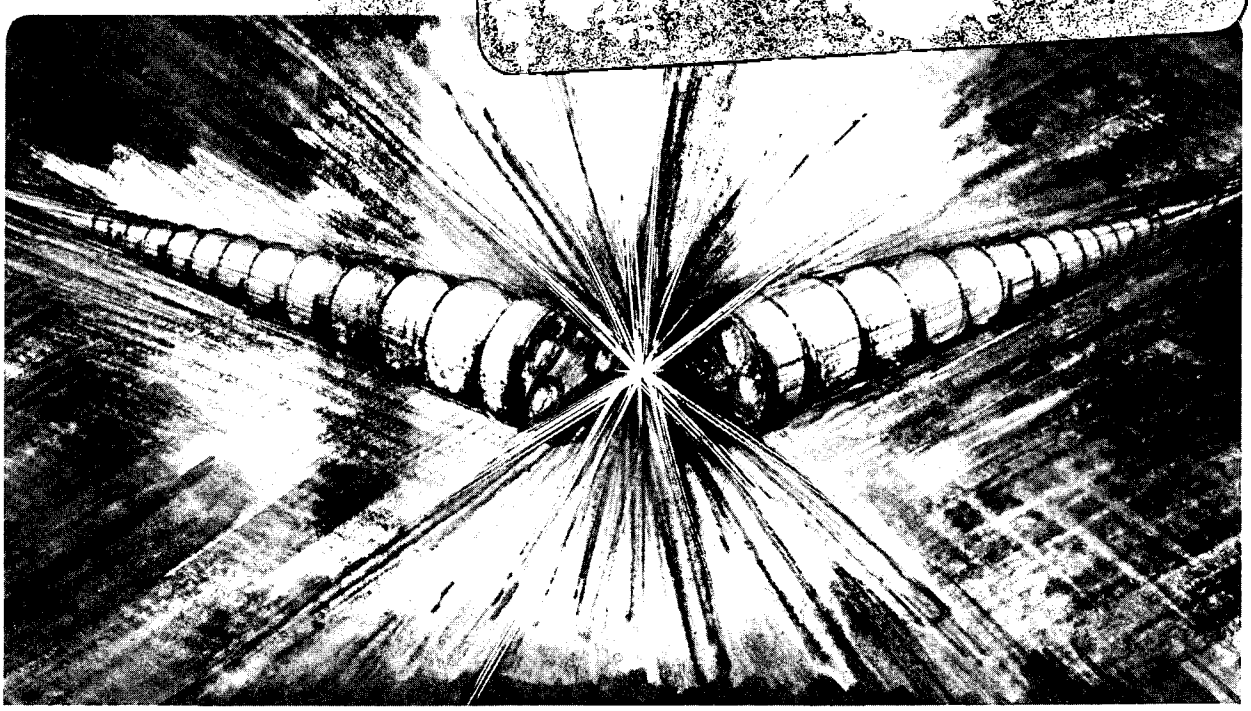

Prepared for the U.S. Department of Energy under Contract DE-AC03-76SF00098

LBL-19501 c.2

DISCLAIMER

This document was prepared as an account of work sponsored by the United States Government. While this document is believed to contain correct information, neither the United States Government nor any agency thereof, nor the Regents of the University of California, nor any of their employees, makes any warranty, express or implied, or assumes any legal responsibility for the accuracy, completeness, or usefulness of any information, apparatus, product, or process disclosed, or represents that its use would not infringe privately owned rights. Reference herein to any specific commercial product, process, or service by its trade name, trademark, manufacturer, or otherwise, does not necessarily constitute or imply its endorsement, recommendation, or favoring by the United States Government or any agency thereof, or the Regents of the University of California. The views and opinions of authors expressed herein do not necessarily state or reflect those of the United States Government or any agency thereof or the Regents of the University of California.

LBL-19501
HIFAN-285

HEAVY ION FUSION HALF YEAR REPORT*

October 1, 1984 - March 30, 1985

Heavy Ion Fusion Staff

Accelerator and Fusion Research

Lawrence Berkeley Laboratory
University of California
Berkeley, CA 94720

June 1985

Attention: This document is provided for DOE "Official Use". Distribution to other interested parties is made with the understanding that no information or experimental results given herein will be quoted without first obtaining the authors' permission, or until such information or results have appeared in the open literature.

*This work was supported by the Office of Energy Research, Office of Basic Energy Sciences, U.S. Department of Energy under Contract No. DE-AC03-76SF00098.

TABLE OF CONTENTS

	Page
HIGHLIGHTS	1
MBE-4: A FOUR-BEAM INDUCTION LINAC EXPERIMENT	3
PERFORMANCE OF THE MBE-4 INJECTOR	4
A DESIGN PROCEDURE FOR ACCELERATION AND BUNCHING IN AN ION INDUCTION LINAC	5
LONGITUDINAL DYNAMICS OF MBE-4	6
TRANSVERSE BEAM DYNAMICS	7
ENVELOPE FUNCTIONS OF A HIGH CURRRENT BEAM	8
ELECTROSTATIC ENERGY ANALYZER	9
LONGITUDINAL BEAM CONTROL	10
A CAPACITIVE BEAM-CHARGE MONITOR FOR SBTE	11
MATERIALS RESEARCH AND DEVELOPMENT	12
Magnetic Materials	12
Insulator Development	12
SIMULATIONS OF ROBERTSON'S LENS	13
SBTE HIGH σ_0 COLLECTIVE STABILITY LIMITS	14

	Page
PUBLICATIONS	15
H.I.F. STAFF ROSTER	18
DISTRIBUTION LIST	19

HIGHLIGHTS

(D. Keefe)

1. The major activity during this reporting period has been the design of the four-beam induction-linac experiment, MBE-4, and the fabrication and installation of the first pieces of this apparatus.

2. The design of MBE-4 has been documented and will appear as a separate report (LBL PUB-5142). We have also documented the progress made on the MBE-16 design which was halted in July 1984, still in an unoptimized form (LBL PUB-5123).

3. The four beam diode injector for MBE-4 has operated successfully at and above its design voltage of 200 kV. Diagnostic devices for all four beams have worked well and show the current and emittance of all beams to be closely the same.

4. To accomplish beam-current amplification requires tailored waveforms at the discrete accelerating gaps. An exact procedure for deriving these now exists, and all the waveforms for a device as small as MBE-4 can be calculaed on an IBM PC for whatever energy/current amplification may be desired. Work is in progress on synthesizing such waveforms in the laboratory, and on evaluating the tolerances in shape, amplitude jitter, and time jitter, that must be maintained.

5. Simulation of the behavior of high-current low-emittance beams in the presence of such real-life effects as image forces and lens misalignments continues to turn up new puzzles, which are slowly being unravelled. Throbbing and growth of emittance can be suppressed by introducing a (usually undesirable) dodecapole component of the right sign in the guide field.

6. An improved matrix method for AG transport of high current has yielded rather simple envelope equations that are accurate to 1% provided σ_0 is less than 90°.

7. Early results from the Single Beam Transport Experiment (SBTE) showed that σ_0 (phase advance per lattice period without space charge) should be chosen to be less than 85° if stable transport of maximum current is desired. No instability thresholds could be identified in such a case. For $\sigma_0 = 60°$ the beam remains stable down to a space-charge depressed phase advance $\sigma = 7°\text{-}8°$, the lowest value possible with the present source. Above $\sigma_0 = 85°\text{-}90°$, an instability threshold could always be detected. An extensive set of measurements for various values of σ_0 above 90° has allowed us to map the stability boundary; a theoretical understanding of the results is, however, still lacking.

8. A 90-degree electrostatic energy analyzer now in place at the end of the SBTE will provide information about the longitudinal beam emittance.

9. In a long ion linac, use of pulsed voltage "ears" from time to time is anticipated to be needed to prevent spreading of the beam at head and tail due to space-charge. A system of such pulses at several discrete locations have been installed in the SBTE. They have been found to keep the bunch end together very successfully.

10. R and D on ferromagnetic and insulating materials beyond the immediate needs of MBE-4 unfortunately has had to be kept to a minimal level. Tests on several formulations of castable epoxy insulators continue to be encouraging.

11. Experiments with the Robertson lens experiment ended in this period; the injector was needed for re-use as the MBE-4 injector. Analysis is proceeding with the help of the MASK code; non-zero electron temperature can be included by this means.

MBE-4: A FOUR-BEAM INDUCTION LINAC EXPERIMENT

R.T. Avery and D. Keefe

We have begun fabrication and installation of the MBE-4 experimental apparatus. The origin of this experiment and the nature of its goals were discussed in the year-end report for FY 1984,[1] and the current design concept is fully described in a separate report.[2] Installation of the apparatus will proceed in stages, interspersed with periods of experimental measurements. While the completion of the intended apparatus is not expected to occur until late in FY 1986 -- given current budget estimates -- we expect a steady flow of experimental information to emerge in the meantime. In fact, reference to Warwick's report in this document[3] will show that this has already begun.

MBE-4 is designed to study induction acceleration and simultaneous current amplification in conjunction with transverse-focussing of four space-charge-dominated heavy-ion (cesium) beams, and to assess electrical/mechanical tolerances needed to avoid emittance growth. The principal parameters (a more extended list is given in Ref. 1 and 2) are:

Injection Current per Beam	(mA)	5-10
Final Current per Beam	(mA)	20-40
Injection Energy	(keV)	200
Final Ion Energy (variable)	(keV)	to 1000
Injection Pulse Duration	(μsec)	2-3

In this reporting period, the overall mechanical design has been completed,[2] and is shown diagrammatically in Fig. 1. The accelerator apparatus consists of 24 accelerating gaps across which the induction voltages appear. The insulators at the accelerator gaps are of Re-X glass-ceramic with cast-in-place metal end-rings, and are on order from GE. Thirty-four quadrupole doublet units, each made up of a pair of nine-electrode electrostatic lens arrays, keep all four beams focussed (see Fig. 2). Fixtures to align the electrodes precisely have been made and tested.

The four beams are produced from four cesium-zeolite buttons and accelerated to 200 keV across a single diode gap in the injector; this entire system has been completed and successfully tested.[3] At present under fabrication is the Beam-Conditioning Unit, immediately downstream of the injector, which will contain eight quadrupole arrays (each with individual voltage control) and extensive diagnostic devices to aid in obtaining a correctly matched and steered beam for transfer to the succeeding Accelerating Sections.

References

1. HIFAR Year-End Report, FY 1984, LBL Report No. 18840 (Dec. 1984).
2. R.T. Avery (for HIFAR Group), LBL Report PUB-5142 (Mar. 1985).
3. A.I. Warwick, see this Report.

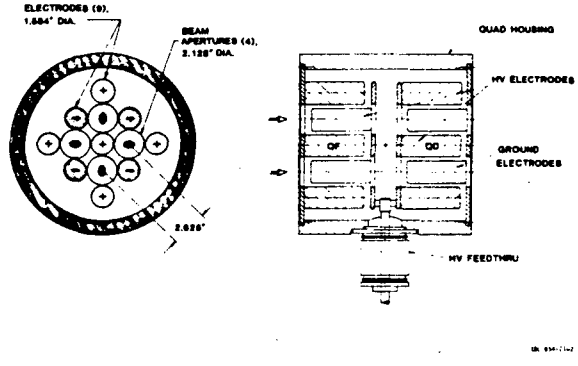

Fig. 2. Transverse and Longitudinal Cross-Sections of a Four-Beam Electrostatic Quadrupole Doublet

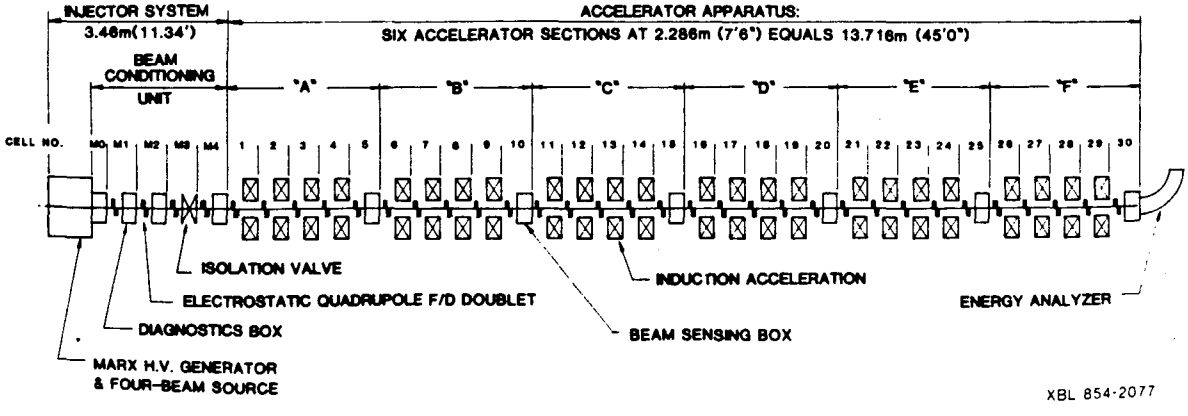

Fig. 1: MBE-4 Diagrammatic Layout

PERFORMANCE OF THE MBE-4 INJECTOR

A.I. Warwick

Construction of the MBE-4 injector was completed in March 1985. First operating experience indicates that the design specifications are met, four beams have been extracted and measured for their current, emittance and time dependence.

Figure 1 shows the injector configuration, this is known as MBE-4 phase 1B.

Four alumino-silicate cesium emitters 1.5 inches in diameter are employed in the fourfold diode. At 200 kV diode voltage these surfaces emit 2 mA cm^{-2} of Cs^+ ions. A shaped graphite electode at 200 kV focusses the four beams through holes in the ground plane plate, the beams do not pass through any grids. Each beam has 20 mA of current and is of uniform current density except for an aberration at the edge. Emittance measurements at this point give a value of the normalized emittance of 1.2x10-7 π m rad. where the emittance is defined by

$$\pi\varepsilon \equiv 4\pi\beta\gamma\left[\langle x^2\rangle\langle x'^2\rangle - \langle xx'\rangle^2\right]^{1/2}$$

At the diode exit the beams can be steered by an array of electrodes. The array geometry is designed to give a uniform transverse impulse to the beams as they pass, the amplitude and direction of which can be varied independently for the four beams. Typically a few milliradians of deflection is required at this point to correct misalignment errors in the diode.

Immediately downstream of the steering array, a collimating aperture intercepts the edges of the beam allowing only the uniform centre to pass through. By this means the beam current injected into the linac can be varied, taking advantage of the possible reduction of emittance when smaller currents are required. Electrons are produced copiously at this interception point. Electostatic guard rings on the steering array, which are used to terminate the steering fields longitudinally, are biased to -3 kV to prevent the electrons from neutralizing the beam upstream of the collimators. It was found that without this bias the beam becomes progressively neutralized on a microsecond timescale, causing time dependent transmission through the collimators.

Emittance measurements have been made 50 centimetres downstream of the collimators, for a 5 and a 15 mA transmitted beam. The normalized values obtained were 1.2x10-7 and 2.0x10-7 π m rad respectively. The emittance of the full 20 mA beam appears to have increased somewhat, presumably due to evolution of the phase space distribution, and is reduced to the quoted values by collimation.

The time structure of the 5 mA beam is shown in Fig. 2. the top trace is the diode voltage, approximately representing the beam kinetic energy, the lower trace is beam current.

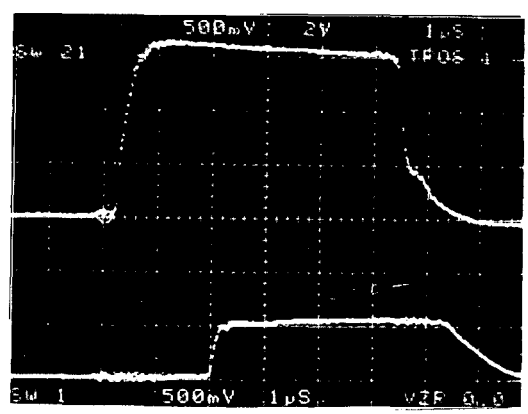

XBB 856-4709

Fig. 2. Voltage and Current from One of the Four Beams

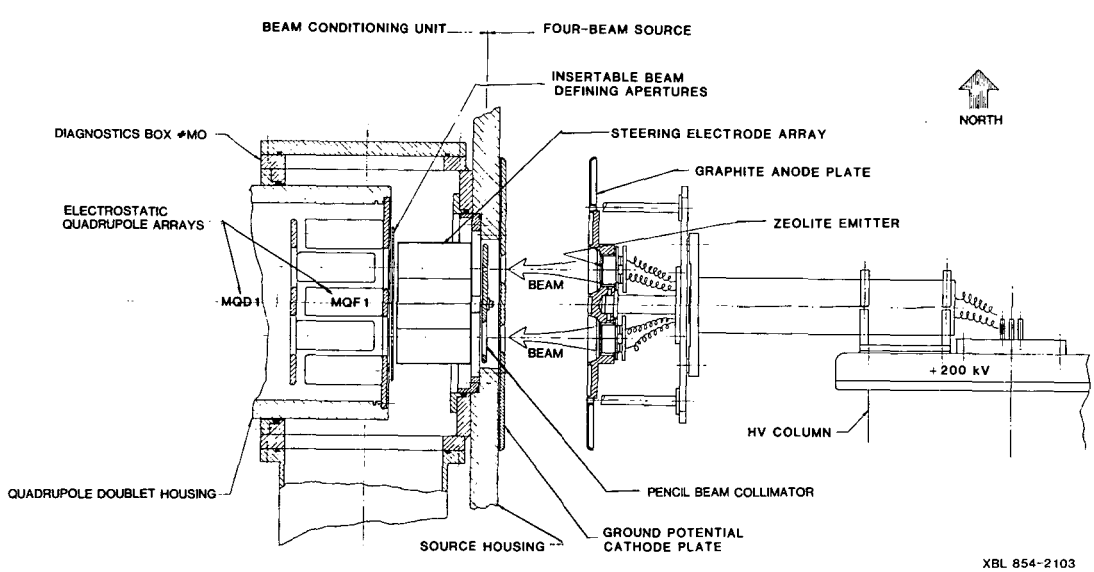

Fig. 1. MBE-4 Injector System

A DESIGN PROCEDURE FOR ACCELERATION AND BUNCHING IN AN ION INDUCTION LINAC

C. H. Kim, and L. Smith

In order to realize current amplification in a linear induction accelerator, the modules should accelerate the tail more than the head of the bunch in some programed fashion. The aim is to maintain the line charge density near to the transverse space charge limit, but at the same time to minimize the longitudinal variation of the line charge density in order to minimize longitudinal space charge forces. The current self-replicating scheme provides one convenient way of achieving this aim; in this scheme all the particles emerging from an accelerating gap are headed towards a common focal spot.

There are a number of design constraints of physics and technological nature. The physics constraints are: (1) in the beam entrance region the head must not be accelerated before the tail has entered, (2) at a given location the velocity variation from head to tail of the bunch should not exceed a certain limit. The technological constraints are: (1) the volt-seconds per meter of the core material should not exceed a certain limit, and (2) the voltage break-down limit. These constraints provide enough information to determine the accelerating voltages for the head and tail of the bunch, thus determining the location of the common focal spot for each gap. The accelerating voltage wave form for all the particles is then determined by the current self-replicating scheme.

A computerized design procedure is devised according to the scheme described above. The code calculates the ideal kinetic energies as well as the actually realized kinetic energies of a number of interacting test particles subjected to realistic accelerating voltages and space charge forces. The difference between the ideal and the realized kinetic energies gives the desired gap voltage wave-form. Using this procedure, we have generated reference designs for HTE and MBE-4. More detailed description of the design procedure and an application of the procedure to HTE can be found in Ref. (1). The reference design for MBE-4 is summarized in Figs. 1 through 3. Synthesis of the voltage waveforms by adding several realistic elementary waveforms is described elsewhere in this report.

References

1. C. Kim and L. Smith, LBL-19137 (1985) submitted for publication in Particle Accelerators.

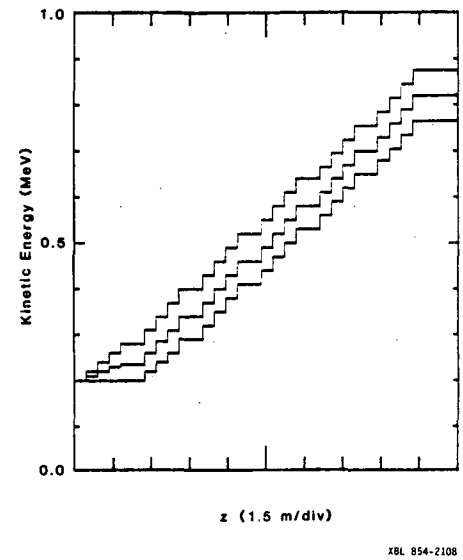

Fig. 1. Kinetic energy of the head, center, and tail of the beam versus z

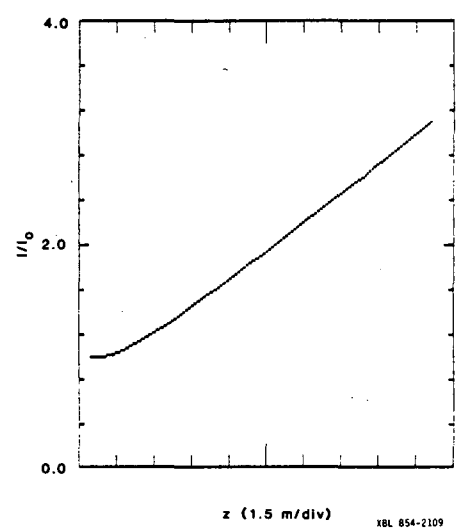

Fig. 2. Normalized current versus z

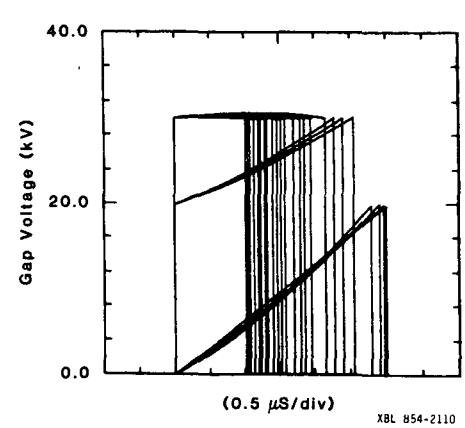

Fig. 3. Ideal wave forms versus t

LONGITUDINAL DYNAMICS OF MBE-4

C.H. Kim, V.O. Brady, T.J. Fessenden, D.L. Judd, and L.J.Laslett

"Ideal" accelerating voltage waveforms of MBE-4, which are described elsewhere in this report, have roughly one of the following typical shapes: (1) a triangular shape in the beam entrance region, (2) a trapezoidal shape in the beam dynamics (db/b) limited and volt-second limited regions, and (3) a flat-top shape in the breakdown limited region. These waveforms were synthesized using the following three types of functions similar to those observed in the development tests:

$$V = V_0 \text{ (constant voltage)} \qquad (1)$$

$$V = V_0\,(2x-x^2); \qquad 0 < x < 1 \qquad (2)$$

$$V = V_0\,(1-\cos(\pi x)); \qquad 0 < x < 2 \qquad (3)$$

where x is the normalized time, $(t-t_0)/t_r$, and t_0 and t_r are the turn-on time and the time to reach the peak voltage, respectively.

MBE-4 will have 30 FODO lattice periods (cells), 24 of which will have an accelerating gap. Every 5-th cell will be used for diagnostic access. The waveforms were synthesized modularly in groups of 4 cells preceding each diagnostic cell. The first three waveforms were synthesized in the simplest way possible. The errors due to the imperfect synthesis and the space charge forces were left to accumulate and then corrected with trimming pulsers at the 4-th cell.

Judgment of the quality of the synthesized waveforms and the beam bunch is somewhat subjective. For HIF applications, the level of fluctuations of the current and the kinetic energy at the exit end of the accelerator have to be within the passband of the final transport system such as the bending magnets and the focusing lenses. Current and energy fluctuations which are reproducible from shot to shot can be corrected in principle to an arbitrary accuracy; however, fluctuations due to the timing and voltage jitters can not be corrected. The effects of jitter depend not only on the magnitude of the jitter but also on the way the waveforms are synthesized. Timing jitters of the individual pulsers on the order 30 nsec introduced current fluctuations of no more than 2%. The magnitude of the fluctuations scaled linearly with the timing jitter.

A total of 71 pulsers was used in the present design study. These waveforms fall into 18 different types which are summarized in Table I.

The calculated kinetic energy, current, and the deviation of the energy from the "ideal" value are shown in Figs. 1(a), (b), and (c). The magnitude of the energy deviation was largely dependent upon the accuracy of the corrections made at the last trimming cell; on the other hand, the magnitude of the current fluctuations was dependent upon the history of the beam acceleration.

TABLE I - MBE-4 Pulsers

Type	V(kV)	t_r(μs)	# Req'd
1	15	-	34
1	10	-	6
2	15	5.0	1
2	15	6.0	3
2	15	6.5	1
2	15	7.0	1
3	7.5	4.2	1
3	7.5	6.0	4
3	5.0	3.0	1
3	5.0	4.0	2
3	3.0	0.9	5
3	5.0	0.9	5
3	3.0	0.5	2
3	0.3	0.6	1
3	0.9	1.3	1
3	3.0	1.5	1
3	2.0	0.5	1
3	5.0	0.6	1
Total			17

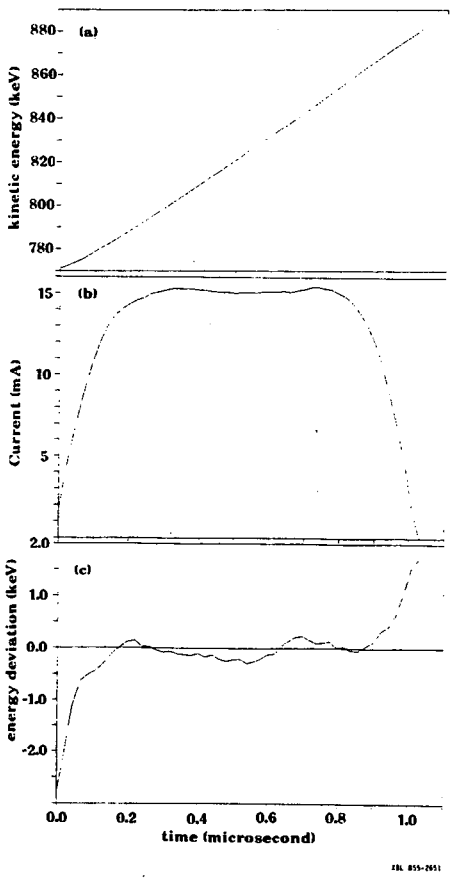

Fig. 1. (a) Kinetic energy, (b) current per each beamlet, and (c) deviation of kinetic energy from the "ideal" value versus time at the exit of MBE-4. At injection each beamlet has 5 mA at 200 keV.

TRANSVERSE BEAM DYNAMICS

C. Celata, L.J. Laslett, L. Smith

Study of the transverse beam dynamics has continued, using the particle simulation code to examine the effects on the beam of charge induced on the conducting electrodes. As described in the last half-year report, the force due to this induced charge (the so-called "image-force") causes no change in the beam dynamics for perfectly aligned beams. For off-axis beams, however, the simulation shows an oscillation and growth of the emittance in both transverse dimensions if $\sigma/\sigma_0 \lesssim 0.1$, as illustrated in Fig. 1 for $\sigma_0 = 60°$, $\sigma = 6°$. (Here σ or

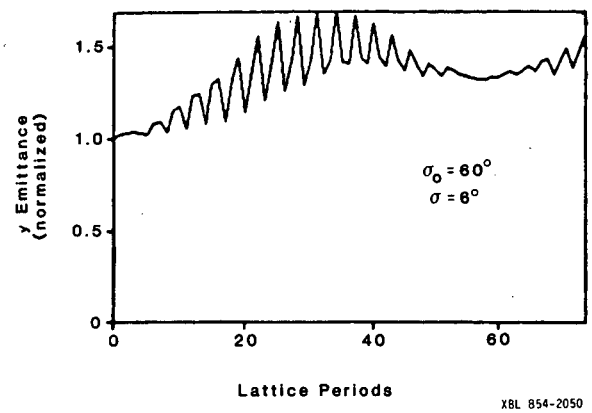

Fig. 1. y-Emittance vs. z with Image Force

σ_0 is the phase advance per period, with or without the space charge force.). The beam size is unaffected by the image forces and the emittance changes are due to transverse heating. The emittance oscillation occurs in a beat pattern caused by the driving of the sextupole mode (frequency just above $\omega_0 = \sigma_0 v_z/2L$, $2L$ = lattice period) by the image forces, which are modulated by the coherent betatron oscillation (frequency just below ω_0). Vlasov analysis of this phenomenon for the case of a beam in a round pipe (image forces caused by the pipe) showed a strong dependence on the pipe radius.

We have now used the simulation to study the effect of shrinking the electrode radius, keeping the electrode centers fixed, thus effectively increasing the "pipe radius". The simulation shows that this does decrease the emittance growth due to the image effect, as expected. For $\sigma_0 = 60°$, $\sigma = 6°$, offset = 2.75 mm, and electrode radius, R_r decreased by 20% from the "magic ratio" value, R_0, the emittance growth was cut by ~ 50%. However, shrinking the electrodes causes a dodecapole field component to occur, which previous study (see the Heavy Ion Fusion Half-Year Report, Oct. 1, 1983 - March 31, 1984) had shown to cause emittance growth. We find using the simulation, however, that the combined effect of the dodecapole and image forces is to suppress emittance growth nearly entirely. This appears to be due to the fact that in the beam frame the dodecapole and image forces both have a sextupole component, but the two occur with opposite signs. This hypothesis is consistent with the fact that changing the sign of the dodecapole force will cause it to enhance, rather than decrease, emittance growth. Figure 2 demonstrates this effect. The case shown is that of Fig. 1, but with the addition of a dodecapole force at the position of each lens. The strength of the dodecapole for the dashed curve is that which would be given by $R_r/R_0 = 0.8$. For the solid curve the sign of the dodecapole field is reversed. For $\sigma_0 = 60°$, $\sigma = 12°$, the growth can be suppressed completely by the dodecapole. We thus believe we have found a method of suppressing emittance growth due to image forces.

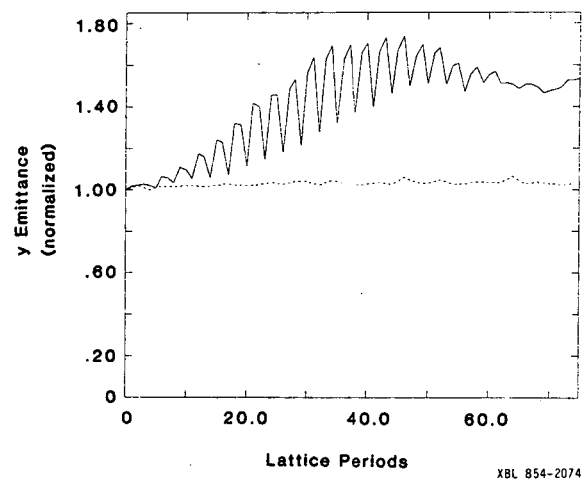

Fig. 2. y-Emittance vs. z with Image Force and Dodecapole Consistent with $R_r/R_0 = 0.8$ (dashed line) and the Negative of This (solid line).

Occurring simultaneously with the emittance oscillation mentioned above is a monotonic growth of emittance which can increase the emittance by a factor ~ 2.5. The magnitude of this emittance growth decreases as the spatial resolution of the particle simulation is increased, and therefore it remains to be determined whether this emittance growth is real. (Note that the sextupole emittance <u>oscillation</u> described above does not change with the simulation spatial resolution, and therefore appears to describe a real effect.) The emittance growth is caused by single particles which appear to be oscillating across the beam at subharmonics of the sextupole mode frequency, and the phenomenon only occurs for off-axis, highly tune-depressed beams in the presence of image forces. There is no evidence for exponential growth due to a numerical instability, and simulation parameters are within what are generally accepted as safe ranges. Study of this phenomenon is continuing.

Other questions currently being studied are the effects of a gross mismatch on transverse beam dynamics, and study of the stability of beams with $\sigma_0 \sim 90°$ and low σ. For the second of these studies, the matching section will be included in the simulation calculation for the first time, as well as a better approximation to thick lens focusing.

For the design of MBE, HTE and a heavy ion ICF driver it is not only necessary to determine the matched beam envelope functions for particular design parameters, but also to provide accurate scale relations and graphical display of the parametric dependences. In general, an exact evaluation of the envelope functions may be obtained from the solution of the nonlinear envelope equation (including space charge), if the K-V distribution is assumed. This has been found to be an adequate theoretical basis for design, but is too cumbersome for the purpose of parametric display and scaling. The well-known continuous limit formulation does yield relations between emittance, current and mean radius, but they are inaccurate (~ ± 30%) and there is no prediction for the maximum radius. These deficiencies of the continuous limit formulas are remedied in an improved approximate calculation described here, while retaining a desired simplicity of form and explicit scaling.

The improved approximation of the envelope functions is based on an evaluation of the transfer matrix [M] for the full lattice period (length 2L). This matrix is the product of the exact matrices for lenses and drifts (without space charge forces), with defocussing lenses representing space charge inserted in the middle of the drifts. At these mid-points the repulsive force is close to its average for the full period and can be evaluated using the mean radius $\bar{a}$. The normal and depressed tunes (σ_0, σ) are determined from the trace of [M] and the ratio $\bar{a}^2(\sin\sigma)/\epsilon$ (where ϵ is emittance) is given by the component M_{12}. The maximum radius $\tilde{a}$ is determined from the transfer matrix evaluated between the center of a focal lens and the center of a drift. In the consideration of thick lenses and treatment of beam charge, this calculation improves on a similar set of results previously derived by Keefe.[1]

The four derived relations essentially relate $\bar{a}$, $\tilde{a}$, σ, and σ_0 to the fundamental quantities: occupancy η, L, ϵ, line charge density (λ), and quadrupole strength (K). To further simplify the relations we expand all trigonometric functions in the dimensionless lens strength ($\eta\sqrt{K}\,L$), keeping the lowest non-trivial contributions to the envelope functions. The formulas for the full period tunes are (for $\eta = 1/2$)

$$\cos\sigma_0 = 1 - K^2L^4/12$$

$$\cos\sigma - \cos\sigma_0 = \Gamma\left[1 - (.225)(1-\cos\sigma_0)\right] + \Gamma^2/8 ,$$

where

$$\Gamma = \frac{\lambda}{2\pi\epsilon_0 E}\left(\frac{L}{\bar{a}}\right)^2$$

is a dimensionless measure of line charge and E is particle energy. These formulas are accurate to within 1% for $\sigma_0 < 90°$. The errors for other quantities are of this order compared with exact results, except $\tilde{a}$, which can be in error by up to 5%.

An example of the application of the approximate envelope formulation is a graph of transportable charge vs. energy for various values of σ_0 and pole tip potential ϕ in the parameter range of MBE and the HTE injector (see Fig. 1).

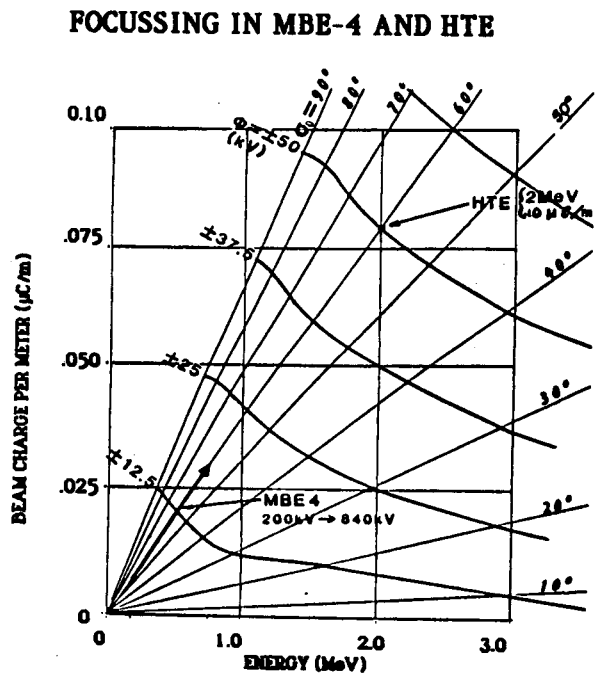

Fig. 1. Transportable Charge vs. Energy for Given Pole Potential, ϕ, and Undepressed Tune, σ_0.

We have assumed $\eta = 1/2$, 50% fill of available aperture radius, and tune is depressed to the equilibrium limit $\sigma = 0$. An additional feature is that the ratio of half period to aperture radius is minimized (L/b = 10, consistent with good field quality) to maximize λ. The rays of constant σ_0 are a guide to stability, with $\sigma_0 < 60°$ a conservative criterion. By increasing injection energy E, the transportable charge is increased along a ray of constant σ_0. This tactic is limited by the allowable voltage on pole faces, which form an essentially orthogonal set of rays in the (E,λ) plane. For MBE's 200 kV injection energy the voltage is only 12.5 kV, however HTE (2 MeV injection) is accomplished with ϕ = 50 kV.

References

1. D. Keefe, HIFAN-7, 1977.

ELECTROSTATIC ENERGY ANALYZER

S.S. Rosenblum and A. Faltens

Until this reporting period the HIF experiments in the various locations have had no precise energy measurement apparatus, and have depended on the discharging voltages on pulsers and on time of flight measurements for determining beam energies. During this period an energy analyzer was designed, constructed, and installed at the end of the SBTE apparatus, where it has already yielded interesting results. The analyzer was designed to achieve 0.1% energy resolution and an acceptance of ± 2.5%. Tests are under way at the present time to tune up the analyzer and measure its resolution. Before the resolution can be measured, the beam stability in the SBTE must be improved somewhat, and very-well-regulated power supplies, which were purchased and have just now been delivered, must be installed on the analyzer.

Initially, magnetic and electric field analyzers were considered, and the electric one chosen because of the much lower cost and easier power supply requirements. The major worry was about beam-induced breakdown, because in the anticipated use on the MBE-4 experiment beam would usually have a very large energy variation from head to tail in the pulse, and most of it would hit the analyzer electrodes. The first tests on the SBTE showed that a 10 microsecond duration, 120 keV, 12mA Cs beam did not cause breakdown up to the maximum voltage of 100 kV across the analyzer gap, while a 100 microsecond long pulse of about 1 mA would cause breakdown down at 30 kV. Evidently the beam is able to initiate some discharge process which may be quite complicated, but that the few-microsecond-long pulses used in the SBTE and the future MBE are not going to be troublesome.

The design of the spectrometer was based on the first order treatment by A.P. Banford.[1] In addition, the formulation of R.E. Warren, J.L. Powell, and R.G. Herb, was used to calculate the focal lengths and resolution.[2] Calculations of the beam orbits were carried out by S. Rosenblum on an I.B.M.-P.C. using Lotus 1-2-3. The field uniformity, aberrations, and electrode geometry were worked on by L.J. Laslett, V. Brady, A. Faltens, and S. Rosenblum. The electrode shape chosen combines a field reducing gradient ring with a slight protrusion into the analyzer gap to increase the good field region. Work by C. Pike is continuing on an electronics system which would be able to sample on a very fast time scale the currents collected by a system of wire collectors in a harp geometry located in the focal plane of the analyzer.

The spectrometer itself is shown in Fig.1. Essentially, it is a pair of flat electrodes bent precisely into an 18" radius arc (coaxial cylinder arcs of 17.5 ins and 18.5 ins with a gap of one inch between electrodes). The resulting 1/r field focuses a 0.5 mm object slit located about 6" in front of the analyzer into, ideally, a 0.5 mm image 6" downstream from the analyzer. The signal to noise ratio of the detector and various aberrations and misalignments will determine the ultimate resolution of the instrument. At the present time the analyzer has already measured the energy distribution in the tails of the bunch, and has discovered an 8.5 MHz energy oscillation of about ± 1% which persists for many microseconds into the pulse but does die out.

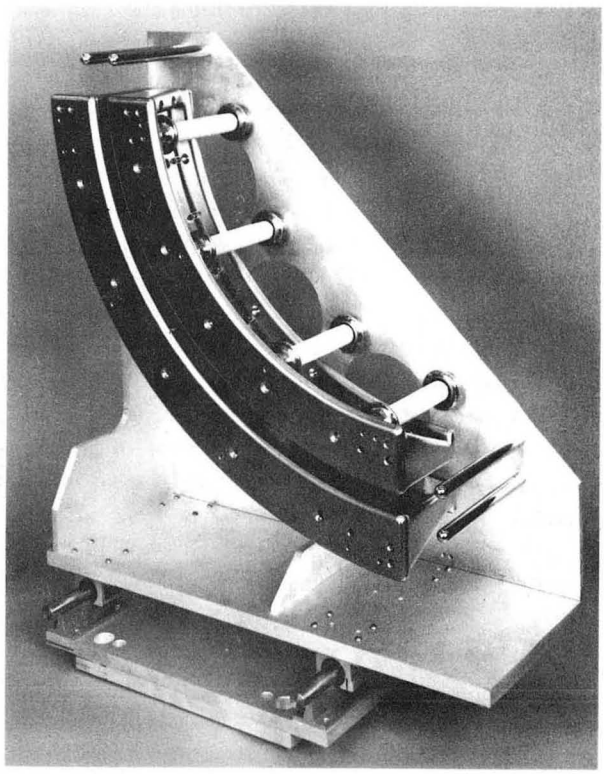

CBB 853-1896

(a)

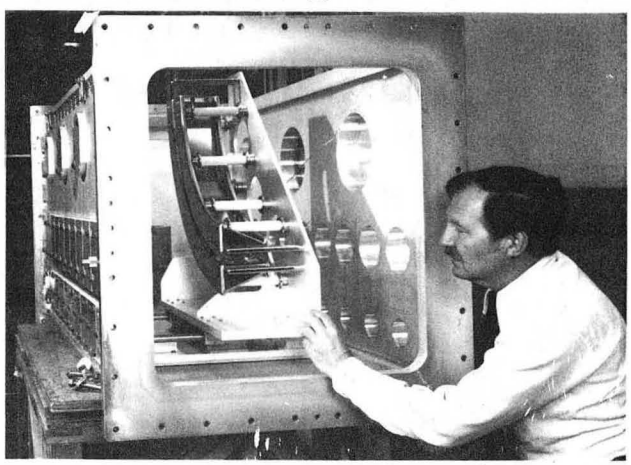

(b) CBB 853-1894

Fig. 1. Electrostatic Analyzer
(a) Close-up of Analyzer, (b) Jurik Shkredka for scale.

References

1. A.P. Banford, "The Transport of Charged Particle Beams", E. and F. Spon, Ltd., London, 1966, p. 84ff.

2. R.E. Warren, J.L. Powell and R.G. Herb, Rev. Sci. Inst., 18, 559 (1947).

A. Faltens

A longitudinal bunch control system designed to work on the tail of the beam bunches in the SBTE was built, installed, and operated. This system is a significant upgrade of the single fast pulser which was used to superimpose a voltage modulation on the gun voltage as reported in the previous half-year report. The new system comprises seven independent pulsers, able to accelerate in drift tube fashion utilizing the beam-enclosing quadrupole structure as shown in Fig. 1, and can be used to keep the rear of the bunch from expanding from the defocusing action of space charge forces. The physics of the main experiment is essentially Newton's First Law: balancing the space charge force arising from the beam with an externally applied restoring force to keep the end of the bunch from moving. Deviations from an ideal balance arise from differences in the solutions of Poisson's Equation and Laplace's Equation, which result in field variations across the transverse dimension of the beam such that the space charge fields are strongest at the edge the beam, and from the application of the restoring forces at 1.8 meter intervals while the beam fields act continuously. The pulsers were made to approximately match the bunch end duration of 0.5 μs seen at the first Faraday cup about 80 cm downstream from the gun. No attempt was made to match the bunch shape to the applied waveform because the accompanying beam energy profile was unknown and unmeasurable at that location, and because the measured current fall, approximating an exponential decay, would require higher voltages and closer timing control than were conveniently available. Instead, the solution chosen here was to provide a 1-exp(-at) type of waveform of sufficient magnitude to act as a very large bucket, in the rf sense, and let the bunch shape adjust to it. The resulting mismatch from these various effects, generated mainly in the earliest pulsers, becomes a space charge wave pulse which propagates into the bunch, while the bunch tail itself reaches a new steady state configuration. Figure 2 shows a long pulse for reference, and a short pulse with and without the longitudinal focusing applied (to the bunch tail only), as measured at the exit of the 13 meter long SBTE quadrupole transport channel. The focusing pushers each provide a 6 kv accelerating pulse with a 0.5 μs risetime and the pulses are applied to the tail with 100 ns timing accuracy at 4.5 μs intervals, in the same intermittent manner which had been contemplated for drivers.

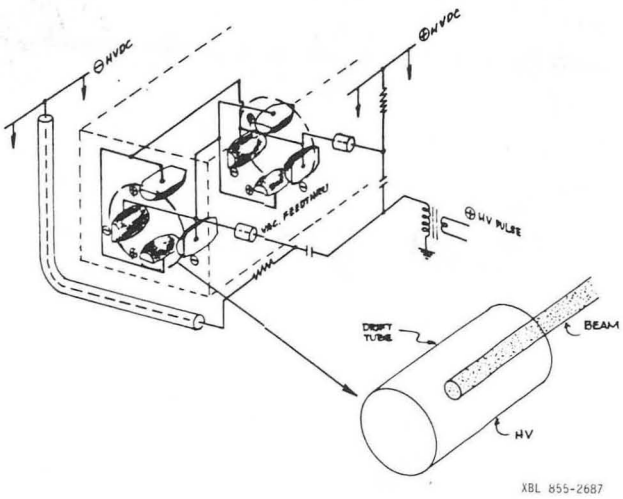

Fig. 1. Quad Pulser Schematic

In addition to keeping the bunch tail together, the new set of pulsers was used to measure the dispersion and large signal behavior of space charge waves on the beam, and the reflection of a short pulse off of the focused and unfocused ends of the bunch, as shown in Fig. 3, where a negative polarity fast current pulse, marked Ref Pulse in the middle of the picture has been advanced into two positions within the front of an unfocused bunch. The accompanying positive polarity slow wave pulses are also seen, having separated from their twins by 2.5 μsec after traveling about 10 meters from their common excitation point. This data is being analyzed, and the time response of the Faraday cup at the end of the machine is being improved, at the present time.

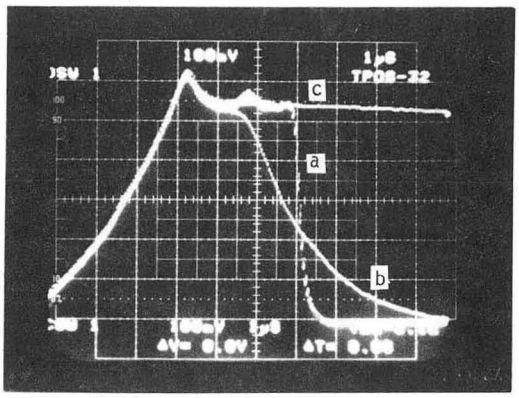

XBB 855-4951 A

Fig. 2. Cs bunch (a) with and (b) without Longitudinal Focusing Applied to the Rear of the Bunch, and (c) a Long Pulse for Reference. The Front is Unfocused in All Three Cases, and Shows Elongation to 4 μsec.

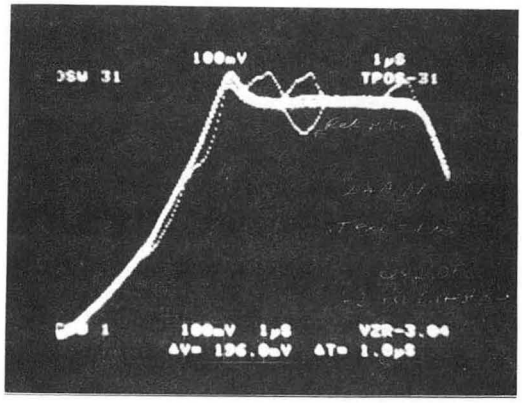

XBB 855-4252

Fig. 3. Propagation of a Short Pulse into the Front of an Unfocused Cs Bunch

A CAPACITIVE BEAM-CHARGE MONITOR FOR SBTE

T.J. Fessenden

During this last period a method of monitoring the charge per unit length of the SBTE beam was developed. The method uses measurements of the charge induced on the quadrupole electrodes by the space charge of the passing Cesium beam. This is a non-intercepting diagnostic that can be used to determine the beam current if the velocity of the beam is known. This diagnostic technique is relatively well known and a general description of the technique can be found in Reference 1.

A diagram of the monitor showing the quadrupole connections and the method of generating the signals is shown in Fig. 1.

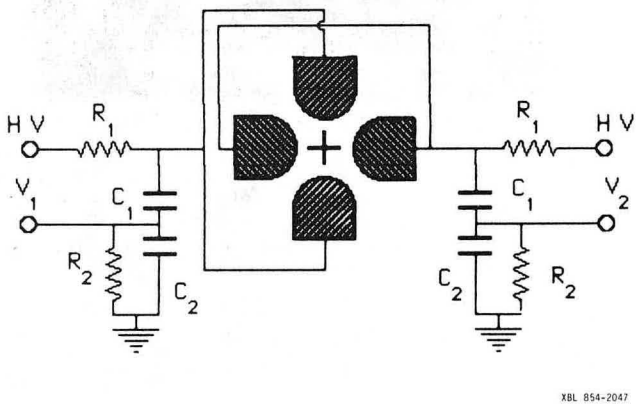

Fig. 1. Circuit Diagram

The focussing voltage for the electrostatic quadrupoles is coupled through the high voltage connection HV. The capacitor C_1 is a blocking capacitor and the capacitor C_2 is the monitoring capacitor. The voltage on C_2 is held near zero by R_2. The various RC time constants are assumed long compared to the time scales of interest. As the unneutralized ion beam passes, a charge Q is induced on the electrodes and in capacitors C_1 and C_2 which causes the voltages V_1 and V_2 to change by an amount $V_{1,2} = Q/C_2$. This charge is related to the beam charge per unit length (q) by:

$$Q \approx qL/2$$

Here L is the effective length of the beam in the quadrupole. If the beam threads the quadrupole, L is estimated to be 95% of the half lattice period for the parameters of SBTE. The rise time of the diagnostic is limited by the beam speed in entering the quadrupole ($\approx$0.3μsec).

Each ion striking the quadrupole electrodes creates between 10 and 15 secondary electrons.(2) Ions striking the positive electrodes eject electrons that are returned to these electrodes by the quad fields. Ions striking the negative electrodes eject electrons that are swept to the positive electrodes. Thus if the electron gain is k, an ion current i striking the negative electrodes causes a current of $i(1+k)$ to flow through the capacitor monitoring circuit connected to this electrode and a current of $-ik$ to flow through the positive electrode monitoring circuit.

Figures 2 and 3 show oscillograms obtained from SBTE quad 47 with a 4.2 mA cesium beam. Figure 2(a) shows the voltages detected on the negative quad electrode pair and Fig. 2(b) shows the voltage detected on the positive quad pair at position 47. Figure 3(a) shows the sum of these voltages which reveals the beam charge versus time. The difference of these voltages, Fig.3(b), shows the electron current generated by local beam spill as integrated by capacitors C_2. If the beam speed is v, the beam current I is given by

$$I = C_2\, v(V_1+V_2)/L$$

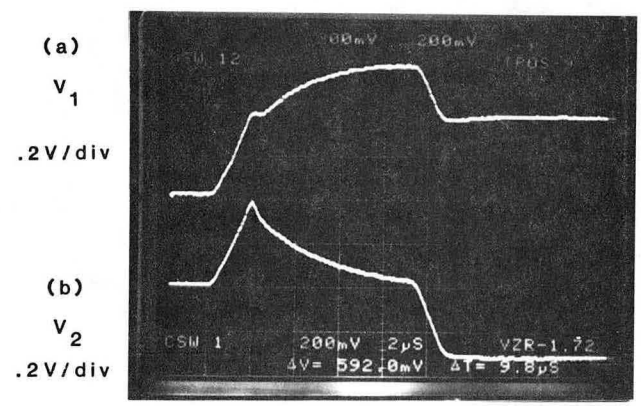

XBB 855-4249 A

Fig. 2. Voltages V_1 and V_2 at Q_{47}
2 μsec/div.

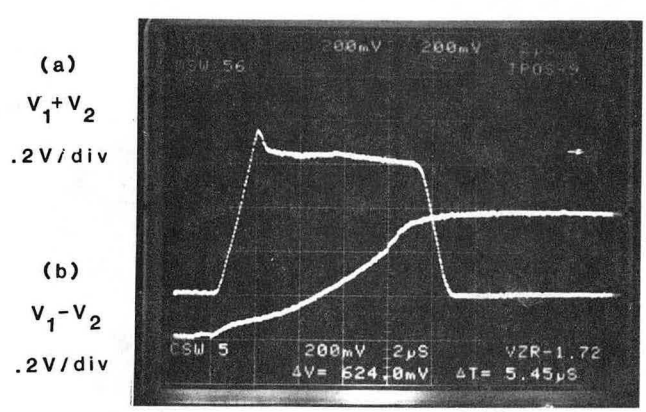

XBB 855-4950 A

Fig. 3. V_1+V_2 and V_1-V_2
2 μsec/div.

References

(1) See for instance J. Borer and R. Jung, DIAGNOSTICS, p. 16, CERN/LEP-BI/84-14, Oct. 1984.

(2) M. Tiefenback, private communication.

Magnetic Materials

R. Astrue, A. Faltens, S. Rosenblum

There are several models which describe the characteristics of magnetic materials under pulsed or ac conditions, such as the "classical eddy current" model, and the "saturation wave" model. These models seldom give more than an approximate indication to what the large signal pulsed behavior of a magnetic material is going to be. To correct or improve upon the simpler models, various mechanisms have been suggested for several decades to account for the so called anomalous losses, but not much can be accomplished without knowing in some detail the dynamics of the domains within the magnetic material. In the case of the various types of magnetic glasses which seem suitable for induction accelerator work, we are not at all sure whether the reversal of magnetization during a pulse is by nucleation of many domains and limited wall motion, or from the motion of one large sandwich domain, or by the rotation of several existing domains.

To add to our meager knowledge, we attempted to freeze the domain pattern in midpulse and to examine the sample with "Bitter Soup". To accomplish this, a crowbar thyratron was added to the core test pulser which would short-circuit the voltage pulse at any point within a typically few microsecond long pulse. By pulsing the core again, we ascertained that some of the volt seconds had been used up and that the core did not reset itself, i.e., the typically square loop materials could be stopped at several places on a hysteresis loop. The domain patterns, however were difficult to see on the surface, and no conclusion could be made. Other domain observation techniques exist which are much faster, and hopefully a similar experiment could be attempted with one of them in the future.

One of the fairly common features of driving induction cores of the square loop type with an approximately flat voltage pulse has been a step of current at the beginning of the pulse, or a step followed by a decrease, as shown in Fig. 1. The "interrupted and frozen" pulse technique shows that the impedance of the core is increasing at first, Fig. 2, and that the decrease of initial current as in Fig. 1 is not simply eddy current decay.

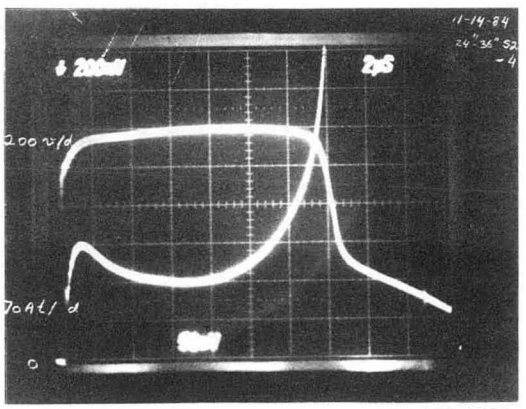

XBB 854-2925

Fig. 1. An example of a fairly common current pulse, bottom, for an approximately flat voltage pulse, top, driving a square-loop core to saturation. Zero for both pulses is at the bottom of the picture.

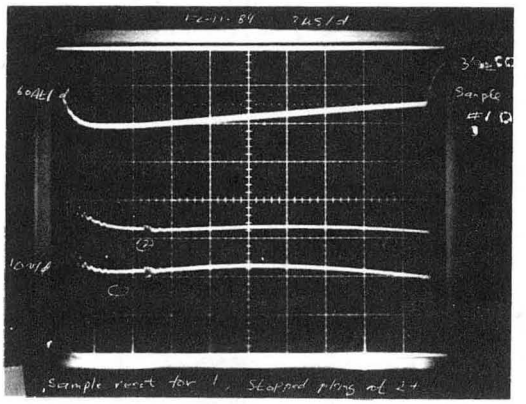

XBB 854-2924

Fig. 2. For almost identical current pulses, top (negative going) applied to an initially reset square-loop core, the voltage generated (positive going) by the first pulse, bottom, and by the second pulse 2. Zero for the voltage pulses is at the bottom of the picture, zero for the current pulses is at the top.

Insulator Development

N. Munshi, S. Rosenblum, A. Faltens, C. Pike

The insulator development program includes evaluation of castable epoxy insulators for various accelerator uses, with the end goal of reducing costs and increasing the availability of large accelerating columns. At the present time, because of budgetary problems, the development of full scale columns has been curtailed, but work is continuing on evaluating small samples for vacuum outgassing, electrical breakdown, and other mechanical properties. Some of the compositions which have been formulated are:

Formulation I, based on a diglycidyl ether of Bisphenol-A epoxy resin, which cures at room temperature and has very low shrinkage;

Formulation IV, based on a cycloaliphatic epoxy resin, which is both hard and tough; and

Formulation VI, with a high impact strength, and is based on a cycloaliphatic epoxy resin incorporating two unique flexibilisers.

While a detailed list of all of their properties is not completed yet, all of the compositions hold 85 kV across a 0.5" long sample, and have outgassing rates in the range of $\times 10^{-9}$ Torr-liters/cm^2 sec., and thus are interesting for further development for induction accelerator use.

SIMULATIONS OF ROBERTSON'S LENS

G. Krafft

Up to the present, theories of Robertson's lens have assumed that the neutralizing electrons are a cold fluid and that the magnetic field in the lens only slightly perturbs the electron density.[1] A linearized perturbation analysis is possible in this case.

Particle-In-Cell simulation calculations were undertaken to study the more general case when electron thermal effects are important and/or when the perturbations are not small. The cylindrically symmetric 2 1/2 dimensional code MASK was used in the simulation work. The major conclusions of the work are:

1) For a given longitudinal velocity and ion density there is an allowed upper limit on the electron temperature. If this temperature is exceeded, nonlinearities in the electric field can destroy the focusing effect. One limit is $\lambda_D < \bar{a}$, where λ_D is the Debye length $(T_e/4\pi e^2 n)^{1/2}$ and $\bar{a}$ is the beam size. In addition one must require $T_e < m\Omega_e^2\bar{a}^2/8$ where Ω_e is the electron cyclotron frequency. Finally if $v_{oz}^2 < v_T\Omega_e\bar{a}$, where v_T is the thermal velocity, some degradation of the field is inevitable and at higher temperatures the nonlinearities get worse.

2) If $v_{oz}^2 > v_T\Omega_e\bar{a}$ the electron distribution evolves to a rigid rotor distribution after the electrons have penetrated the lens.

3) Robertson realized that the magnetic field only slightly perturbs the electron density when $1/2\ \Omega_e^2/\omega_p^2 << 1$, where ω_p is the electron plasma frequency. If this inequality is not satisfied and the beam is surrounded by a grounded conducting cylinder inside the magnetic field, the self-consistent electric field has significant nonlinearities in r.

4) The nonlinearities in the electric field may be reduced by biasing the beam-surrounding conductor positively. In some parameter regimes, the nonlinearities cannot be entirely eliminated in this manner due to heating of the electrons in the large applied fields.

As an example, consider the second conclusion. A rigid rotor distribution is characterized by the fact that the average v_θ increases linearly with r. In Fig. 1 a scatter plot of r vs. v_θ is given for those electrons completely inside the magnetic field. The simulation parameters were $v_{oz} = 3\times10^7$ m/sec, $n_i = 1.5\times10^{16}$ m^{-3}, $T_e = 80$ eV, and $B_z = 400$ G. (These parameters would be appropriate for the final focussing needs of the HTE.) The ion density is chosen to be uniform out to r = 2 cm and a grounded conductor boundary condition is applied at r = 5 cm. The solid line is the rotation velocity if $v_\theta = (\Omega_e/2)r$. Given this evidence that the electrons are rigidly rotating, it is possible to describe the equilibrium when the electrons are inside the lens with a 1-dimensional numerical model. This model requires much less computer time than a full simulation and reproduces the simulation results well.

Simulations of a HTE final focus lens give quite favorable results. If $T_e < 100$ eV, designs with B_z about 400 G are possible. Work at Los Alamos indicates that neutralization of the beam using a bias grid arrangement yields electron temperatures below 100 eV.[2]

The simulations were undertaken in part to explain experimental results. By tracking the ions through the collective electric field computed by simulating the experiment, we find that the results are in better agreement with the experiment than results computed with the linearized theory. (The direct magnetic force on the ions is negligible.)

During the reporting period, experiments on the large contact ionization source were concluded. The final experiments were a measurement of the vertical ion emittance and a focussing experiment at higher ion current.

References

1. S. Robertson, Phys. of Fluids, 26, 1129 (1983).
2. D. Lemons and M. Jones, private communication.

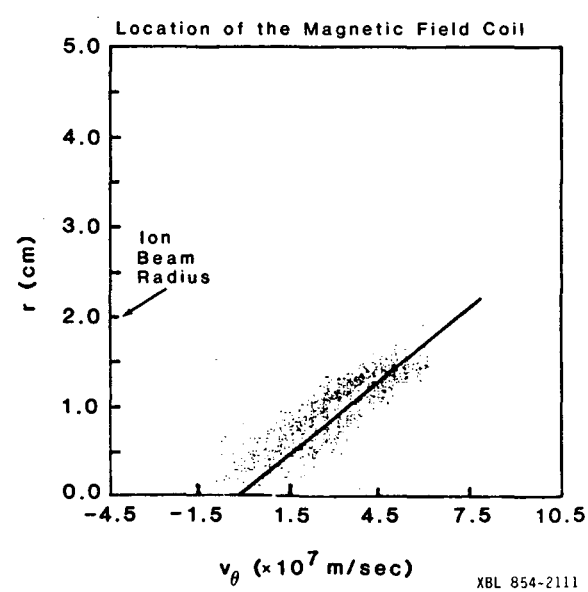

Fig. 1. r vs v_θ Simulation Scatter Plot for the Electrons Inside the Magnetic Field

SBTE HIGH σ_0 HIGH-CURRENT STABILITY LIMITS

M.G. Tiefenback

The Single Beam Transport Experiment (SBTE) was designed to identify beam transport limits relevant to Heavy Ion Fusion (HIF). HIF requires high current beams with low transverse emittance. The SBTE had as one major goal to identify the high space-charge, low transverse emittance limit at which collective effects begin to degrade the emittance.

The SBTE consists of a Cs^+ thermionic source, various beam attenuating and emittance spoiling grids, five quadrupoles for transverse beam matching, 82 quadrupoles in a periodic FODO transport channel, and associated current and emittance diagnostics.[1]

Through Fiscal Year 1984 we made extensive beam measurements, primarily for σ_0 (single-particle betatron phase advance per FODO period) $\leq 90°$,[1] finding no detectable emittance growth for the highest current and lowest emittance obtainable from one source for $\sigma_0 \leq 85°$. Since then we have characterized the definite collective effect threshold for emittance growth for $\sigma_0 > 90°$ lattice conditions.

The data analysis for $\sigma_0 > 90°$ is still in progress, but we can report some results using the following framework. It was noted by Sacherer[2] that the trajectory equation for particles in a beam can be averaged over the distribution to obtain rms radius equations identical in form to the K-V envelope equations. Field nonlinearities are involved in an extra equation determining the evolution of the RMS emittance, but if this quantity is known to be (for instance) constant, the RMS radii of the beam evolve just as the radii of a K-V beam in a linear lattice. While a K-V beam has a unique net σ (phase advance per period with self-field), the real, nonlinear self-field beam has a spread of betatron frequencies. Still, the σ corresponding to a K-V beam with the same current and RMS emittance of a real beam is a measure intensity of, and is some average of the real oscillation frequencies. While this σ value derived from beam current and emittance measurements is most meaningful in the low σ (low emittance) limit, it provides a parametrization of beam intensity for all cases, which we shall use in this report.

In the process of making beam measurements for $90° < \sigma_0 < 105°$, we found that an apparently stable asymptotic beam distribution developed during transport from injecting a beam of too low an emittance for stable propagation. The spontaneously rearranged beam distributions contained a higher current for the same RMS emittance than any we could obtain from the source that would transport stably over even the first 15 periods of the lattice. The σ values derived from the current and RMS emittance for the (apparently) asymptotically stable distribution are shown vs. σ_0 in Fig. 1 as explained in the caption.

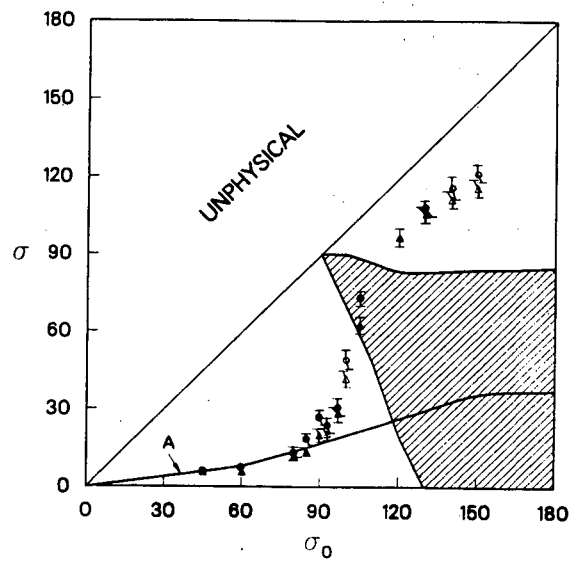

XCG 856-233

Fig. 1. Plotted are calculated σ values for stable and apparently stable beams for various σ_0. Filled-in symbols represent beams with the same current and emittance at the beginning and end of the lattice. Hollow symbols mark σ values derived from beams reproducing ϵ and current over at least the last 10 periods, for $\sigma_0 = 100°$. Circles mark σ values derived using full beam distribution RMS emittance. Triangles mark calculations using central 95% current of the phase space distribution. The shaded region marks the calculated instability of the envelope equations. Curve A marks the region of equivalent σ attainable at injection with our limited source emittance.

The region $\sigma_0 > 90°$ is clearly undesirable for HIF use, but there is no detectable lower bound to the emittance maintainable for a fixed current in an AG lattice for $\sigma_0 < 85°$. The exact point of separation between the two regimes is uncertain.

References

1. W. Chupp et al., Proc. 1984 INS International Symposium on Heavy Ion Accelerators and Their Applications to Inertial Fusion (Tokyo), Jan. 23-27, 1984, pp. 860-869.

2. F.J. Sacherer, CERN internal report SI/DL/70-12 and Proc. 1971 Particle Accel. Conf., IEEE Trans. on Nuc. Sci., NS-18 (3), 1105-1107 (1971).

PUBLICATIONS

HI-FAN-264	V. Brady	Harmonic Analysis of the Electrostatic Potential due to an Array of Not Necessarily Round Rod Quadrupoles for Focusing Four Beams. (11/84)
HI-FAN-265 LBL-18840	HIF Staff	Heavy Ion Fusion End of the Year Report (April 1, 1984 - September 30, 1984)
HI-FAN-266	S.S. Rosenblum (trans.)	Partial Translation of Section 15, Chapter I pp. 80-84 of Electrische Hochstspannung/A. Bouwers, Berlin (12/84)
HI-FAN-267	L.J. Laslett	Additional Computed Parameters for Periodic-Solenoid Trasnport Lattice Sequel to HI-FAN of January 1983. (12/84)
HI-FAN-268 LBID-1004	L. Smith	Sextupole Mode Driven by a Coherent Beam Oscillation (2/85)
HI-FAN-269	H.H. Heckman, H.R. Bowman Y.J, Karant, J.O. Rasmussen,A.I. Warwick and Z.Z. Xu	Range-Energy Relation for Au Ions, $\leq$ 152 MeV/amu. (3/85)
HI-FAN-270	E.P. Lee	Heavy-Ion Fusion System Assessment Project/Quarterly Status Report, Sept - Dec. 1984. (3/85)
HI-FAN-271	L. Jackson Laslett	"The Image-Field Potential of a Uniformly Charged Ellipse Situated Between a Set of Conducting Hyperbolic Surfaces". Addendum to HI-FAN-117 (3/85)
HI-FAN-272 LBL-19137	C.H. Kim and L. Smith	A Design Procedure for Acceleration and Bunching in an Ion Induction Linac (To be published in Particle Accelerators) (3/85)
HI-FAN-273 LBL-19601	D. Keefe	Developments in Accelerators for Heavy Ion Fusion Abstract for 1985 Particle Accelerator Conference, Vancouver, B.C., May 13-16, 1985 (1/85)
HI-FAN-274 LBL-19487	A.I. Warwick	A Four-Beam Cesium Injector for MBE-4 Abstract for 1985 Particle Accelerator Conference, Vancouver, B.C., May 13-16, 1985 (1/85)

HI-FAN-275 LBL-19560	E.P. Lee T.J. Fessenden	Transportable Charge in a Periodic Alternate Gradient Systems Abstract for 1985 Particle Accelerator Conference, Vancouver, B.C., May 13-16, 1985 (1/85)
HI-FAN-276 LBL-19526	A. Faltens S. Rosenblum	Investigation of Re-X Glass Ceramic for Accelerator Insulating Columns Abstract for 1985 Particle Accelerator Conference, Vancouver, B.C., May 13-16, 1985 (1/85)
HI-FAN-277 LBL-19602	E.P. Lee	The High Temperature Experiment; Choice of Parameters Abstract for 1985 Particle Accelerator Conference, Vancouver, B.C., May 13-16, 1985 (1/85)
HI-FAN-278 LBL-19647	M.G. Tiefenback D. Keefe	Minimum Steady-State Emittance to Current Ratio for Alternating Gradient Transport of Charged Particle Beams Abstract for 1985 Particle Accelerator Conference, Vancouver, B.C., May 13-16, 1985 (1/85)
HI-FAN-279 LBL-19485	C.M. Celata I. Haber L.J. Laslett L. Smith M.G. Tiefenback	The Effect of Induced Charge at Boundaries on Transverse Dynamics of a Space-Charge-Dominated Beam Abstract for 1985 Particle Accelerator Conference, Vancouver, B.C., May 13-16, 1985 (1/85)
HI-FAN-280 LBL-19620	R.T. Avery C.S. Chavis T.J. Fessenden D.E. Gough T.F. Henderson D. Keefe J.R. Meneghetti C.D. Pike D.L. Vanecek A. Warwick	MBE-4, A Heavy Ion Multiple-Beam Experiment Abstract for 1985 Particle Accelerator Conference, Vancouver, B.C., May 13-16, 1985 (1/85)
HI-FAN-281 LBL-19563	C. Kim V.O. Brady T.J. Fessenden L.J. Laslett D. Judd L. Smith	Synthesis of MBE-4 Accelerating Waveforms Abstract for 1985 Particle Accelerator Conference, Vancouver, B.C., May 13-16, 1985 (1/85)

HI-FAN-282 LBL-19484	A. I. Warwick D. Vanecek O. Fredriksson	A Four-Beam Cesium Injector for MBE-4 Abstract for 1985 Particle Accelerator Conference, Vancouver, B.C., May 13-16, 1985 (1/85)
HI-FAN-283 LBL-19527	C.M. Celata V. Brady I. Haber L.J. Laslett L. Smith	The Effect of Focusing Field Nonlinearities in MBE-4 on Transverse Beam Dynamics Abstract for 1985 Particle Accelerator Conference, Vancouver, B.C., May 13-16, 1985 (1/85)
HI-FAN-284 LBL-19529	G.A. Krafft C.H. Kim L. Smith	The LBL Neutralized Beam Focusing Experiment Abstract for 1985 Particle Accelerator Conference, Vancouver, B.C., May 13-16, 1985 (1/85)

H.I.F. STAFF ROSTER

Denis Keefe

Robert T. Avery
D. Brodzik
Clarence Chavis
Warren Chupp
Edwin R. Edwards
Andris Faltens
Thomas J. Fessenden
David Gough
Edward C. Hartwig
T. Henderson
Charles H. Kim
John Meneghetti
N. Munshi
Chester D. Pike
Stephen S. Rosenblum
Gerald L.Stoker
Michael Tiefenback
David Vanecek
Anthony Warwick

Lloyd Smith

Joseph Bisognano
Victor Brady
Christine Celata
D.L. Judd
Geoffrey Krafft
L. Jackson Laslett
Edward P. Lee

William B. Herrmannsfeldt, SLAC

H.I.F. HALF-YEAR REPORT: DISTRIBUTION LIST

Allied Chemical Corporation

Carl Smith

Argonne National Lab.

Thomas A. Fields
Ronald Martin

University of Arizona

R. Morse

Batelle

John Hartman

Bechtel

W. Allen

Brookhaven National Lab.

Mark Barton
E. Courant

C.E.A. Bruyeres-le-Chatel

R. Dei-Cas

University of Calif., Irvine

Norman Rostoker

Cornell University

John Nation
Ravi N. Sudan

DARPA

Joseph Mangano

Department of Defense (SDIO)

Richard Gullickson
Gerold Yonas

Department of Energy

DP-OIF

Sheldon L. Kahalas
L. Killion
R. Schriever
Marshall Sluyter
Col. Charles Whited

ER

Terry Godlove (HENP)
James Leiss (HENP)
Gerry Peters (HENP)
Robert Rader (OPA)
D. Stevens (BES)
David F. Sutter (HENP)
Alvin Trivelpiece, Dir.,
Office of Energy Research
William Wallenmeyer (HENP)

DoE San Office

Rudolf Bredderman
Dennis Neely

E.P.R.I.

Robert Scott

Fermi National Accelerator Lab.

Frank T. Cole
Fred Mills
Lee Teng

F.O.M. Amsterdam

F. Siebenlist

GANIL

P. Lapostolle

GE

John Lucek

GSI

R. Bock
D. Boehne
I. Hofmann

University of Illinois

G. Miley

Institute for Nuclear Study

Y. Hirao

KMS Fusion, Inc.

Alex Glass
Michael J. Monsler

Kanazawa University

S. Kawasaki

Lawrence Berkeley Laboratory

R. Avery, 46/189
K. Berkner, 50/149
J. Bisognano, 47/112

Lawrence Berkeley Laboratory (cont'd)

C. Celata, 47/112
W.W. Chupp, 47/112
T. Elioff, B46B
A. Faltens, 47/112
T. Fessenden, 47/112
A. Garren, 47/112
D. Gough, 47/112
H. Grunder, 50A/4119
E. Hartwig, 47/112
H. Heckman, 50/245
T. Henderson, 46/161
E. Hoyer, 46/187
E. Hyde, 50A/4133E
R. Johnson, 50A/4119
D. Judd, 47/112
D. Keefe, 47/112
C. Kim, 47/112
G. Krafft, 47/112
M. Krebs, 50A/4112
W. Kunkel, 4/230
G. Lambertson, 47/112
L.J. Laslett, 47/112
E.P. Lee, 47/112
E. Lofgren, 47/112
J. Marx, 50/149
J. Meneghetti, 46/161
J. Peterson, 90/4040
A. Sessler, 4/230
D. Shirley, 50A/4113
L. Smith, 47/112
C. Taylor, 46/161
M. Tiefenback, 47/112
D. Vaughan, 50/149
A.I. Warwick 47/112

Lawrence Livermore Laboratory

Roger Bangerter, L-477
Richard J. Briggs, L-321
John L. Emmett, L-488
John Holzrichter, L-481
William Krupke, L-488
Jim Mark, L-477
John Nuckolls, L-477
Louis Reginato, L-526
Erik Storm, L-481

Lockheed

John Siambis

Los Alamos National Laboratory

Ihor Bohachevsky
Richard Cooper
Robert Jameson
Don Kerr
Edward Knapp
Earl Meyer
Roger B. Perkins
Steve Rockwood
Henry Rutkowsky
Richard Stokes
Tai-Sen Wang
Doug Wilson

University of Maryland

Martin Reiser
Derek Tidman

Max Planck Inst. fur Plasma Physik Garching

Arnulf Schluter

Maxwell Laboratories

Library

National Bureau of Standards

S. Penner
M. Wilson

Naval Research Lab.

Steven Bodner
T. Coffey
Irving Haber
Philip Sprangle
Peter Turchi

Occidental Research Corp.

Wyn Salisbury

Osaka University

T. Mochizuki
C. Yamanaka

Universita di Padova

A. Pascolini
M. Pusterla

Physical Dynamics

G. H. Gillespie

Physics International

Library

Pulse Sciences, Inc.

Ian Smith
Ken Riepe

RAFAEL

Joseph Shiloh

Rutherford Laboratory

John D. Lawson
Chris Pryor

Sandia Laboratories

Everet H. Beckner
Don Cook
Glenn Kuswa
Tom Martin
J.P. Vandevender

Soka University

Tetsuya Saito

SOREQ Nuclear Research Center

A. Sternlieb

SLAC

William Herrmannsfeldt, Bin 26
Burton Richter, Bin 7

TRW

J. Gordon
Z. Guiragossian
J. Maniscalco
A.W. Maschke
W. Steele

University of Texas at Austin

Toshi Tajima

Varian

S.S. Rosenblum

Westinghouse

M. Nahemow
E. W. Sucov

University of Wisconsin

G. Kulcinski
G. Moses
R. Peterson

This report was done with support from the Department of Energy. Any conclusions or opinions expressed in this report represent solely those of the author(s) and not necessarily those of The Regents of the University of California, the Lawrence Berkeley Laboratory or the Department of Energy.

Reference to a company or product name does not imply approval or recommendation of the product by the University of California or the U.S. Department of Energy to the exclusion of others that may be suitable.

LAWRENCE BERKELEY LABORATORY
TECHNICAL INFORMATION DEPARTMENT
UNIVERSITY OF CALIFORNIA
BERKELEY, CALIFORNIA 94720